Journal of Materials Chemistry C

Accepted Manuscript

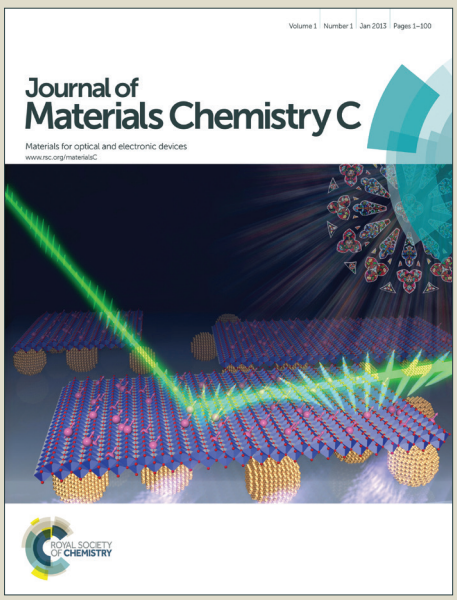

ROYAL SOCIETY OF CHEMISTRY

www.rsc.org/materialsC

J. Mater. Chem. C Journal of Materials Chemistry C Dynamic Article Links ►

Cite this: DOI: 10.1039/c0xx00000x

www.rsc.org/xxxxxx

PAPER

Morphology controlled synthesis of wurtzite ZnS nanostructures through simple hydrothermal method and observation of white light emission from ZnO obtained by annealing the synthesized ZnS nanostructures

Arup Kanti Kole,[a] Chandra Sekhar Tiwary [b] and Pathik Kumbhakar*[a]

Received (in XXX, XXX) Xth XXXXXXXXX 20XX, Accepted Xth XXXXXXXXX 20XX
DOI: 10.1039/b000000x

A controllable synthesis of phase pure wurtzite (WZ) ZnS nanostructures have been reported in this work at a low temperature of ~220^{0}C by using ethylenediamine as the soft template and by varying the molar concentration of zinc to sulphur precursor as well as by using different precursors. A significant reduction in the formation temperature required for the synthesis of phase pure WZ ZnS has been observed. A strong correlation between the morphology of the synthesized ZnS nanostructures with the precursors used during synthesis has been observed. It has been found from Scanning Electron Microscope (SEM) and Transmission Electron Microscope (TEM) image analyses that the morphology of the ZnS nanocrystals changes from sheet-like to belt-like structure having average length of ~450 nm when the molar ratio of zinc to sulphur source is increased from 1:1 to 1:3. An oriented attachment (OA) growth mechanism has been used to explain the observed shape evolution of the synthesized nanostructures. The synthesized nanostructures have been characterized by X-ray diffraction technique as well as by UV-Vis absorption and photoluminescence (PL) emission spectroscopies. The as-synthesized nanobelts exhibit defect related visible PL emission. On isochronal annealing of the nanobelts in air in the temperature range of 100^{0}C-600^{0}C, it has been found that white light emission with a Commission Internationale de I'Eclairage 1931 (CIE) chromaticity coordinate of (0.30, 0.34), almost close to that of white light (0.33,0.33), can be obtained from ZnO nanostructures obtained at the annealing temperature of 600^{0}C. UV light driven dye degradation of methyelene blue (MB) dye aqueous solution has also been demonstrated by using as-synthesized nanobelts and ~98% dye degradation has been observed only within 40 min. of light irradiation. The synthesized nanobelts with visible light emission and having dye degradation activity can be effectively used in future optoelectronic devices and in water purification for cleaning of dye.

1. Introduction

Semiconductor nanorods and nanowires, representing a class of quasi-one dimensional (1D) nanostructures, have attracted considerable attention of researchers since the last few years because of their novel physical properties.[1,2] These 1D semiconducting nanomaterials are playing important roles in mesoscopic research, development and fabrication of nanodevices[1-5] and fabrication of various kinds of semiconductor nanowires and nanorods, nanobelts have been reported by utilizing different methods.[6-8] It has been demonstrated by earlier researchers that the electronic, linear and nonlinear optical (NLO) properties of these nanomaterials are extremely dependent on their morphologies (including size, shape, dimension and composition).[9-12] Considering these facts in mind, it is extremely important to finely control and tune the morphologies of the nanostructures for specific applications of interest by carefully controlling the parameters that affects their growth.

Zinc sulphide (ZnS) is one of the extremely important II-VI wide direct bandgap semiconductors having novel fundamental optoelectronic properties.[1-4] ZnS finds it diverse applications in ultraviolet light emitting diodes (LEDs), flat-panel displays, electroluminescent devices (ELDs), sensor, laser, photocatalysis, infrared (IR) windows etc.[1-5] For manipulation of optical and electronic properties, tuning of the morphology during synthesis is required. Different methods have been used in the past for the controllable synthesis of ZnS nanostructures, such as nanoparticles, nanowires, nanorods, nanobelts, nanosheets and various hierarchical nanostructures.[1-10] One-dimensional (1D) nanowires or nanorods and two-dimensional (2D) nanosheets and nanobelts of ZnS showed interesting optical and electronic properties. Therefore, the research efforts in the field of morphology control synthesis of ZnS have been mostly focused with an aim to fabricate these nanostructures.[6-10] Further, it is well known that ZnS exists in two different polymorphic phases, namely cubic zinc blende (ZB) and hexagonal wurtzite (WZ)

phases.[1, 11-13] Among these, at room temperature the ZB structure of ZnS is the most stable form in bulk, while the WZ phase is a thermodynamically metastable state formed at a very high temperature of 1020°C and melts at 1650°C [13] and there is a free-energy difference of ~13 kJ mol^{-1} between the ZB and WZ forms at ambient conditions.[12] It is desired to have a WZ ZnS structure due to its excellent optical properties than those of ZB ZnS structure, as indicated earlier.[12]

Out of various methods available for the synthesis of ZnS nanostructures, the hydrothermal method has been widely used as a facile and effective low temperature method to synthesize the WZ ZnS nanostructures.[3,5,12-19] In some earlier reports of hydrothermal synthesis of ZnS, ethylenediamine (en) has been used as a molecular template,[15-18] which has also been widely used to synthesize many other kinds of nanoscale materials. ZnS nanocrystals with various morphologies including nanospheres, nanorods, nanowires and nanosheets have been synthesized by using en as the reaction medium.[3,5,13-18] In case of en assisted synthesis, en molecules react with Zn and S to form intercalated lamellar compound $ZnS(en)_{0.5}$ acting as the structure directing agent for the growth of the nanostructures.[5,12,16-17] But in order to obtain pure WZ ZnS structures from these compounds usually a post annealing treatment or post hydrothermal treatment is required to remove the en molecules.[5,15-18] Deng *et al.*[16] prepared phase-pure hexagonal WZ ZnS by annealing the $ZnS(en)_{0.5}$ precursors in argon atmosphere and at above 350°C temperature. Nasi *et al.*[17] have reported the synthesis of porous WZ ZnS and ZnO nanoplates by annealing the $ZnS(en)_{0.5}$ precursors at the temperature range of 400^0C-600^0C in air. Recently, we have also reported the synthesis of WZ ZnS nanoplates by simple annealing the complex $ZnS(en)_{0.5}$ precursors in air at 400^0C temperature.[18] It is still challenging to synthesize directly phase pure WZ ZnS by hydrothermal method and can be done only by finely controlling the different parameters, such as temperature used during synthesis, by using different precursors as well as by changing precursor ratio etc.

However, in this study we have attempted a controllable synthesis of various nanostructures of ZnS and also achieved synthesis of direct phase pure WZ ZnS nanostructures by simple hydrothermal method at a temperature as low as 220^0C. The effect of variation of the molar ratio of zinc to sulphur precursor has been studied and it has been found that with a lower sulphur concentration block-like and belt-like nanostructures are produced, whereas with a higher concentration of sulphur source, belt-like ZnS nanostructures of ~450 nm in (average) length and of ~10-20 nm in width are obtained. The as-synthesized nanobelts are consisting of phase pure WZ structure of ZnS and with preferential growth along the [001] direction. The strong polarity of the (001) plane composed of Zn cations or S anions drives the oriented attachment (OA) of ZnS nanocrystals (NCs) along this direction via electrostatic (or dipole) interaction. Further, we have also studied the effect of using different zinc and sulphur precursor materials on the morphology of prepared ZnS nanostructures but by keeping the molar ratio constant. It is seen that cuboid and spheroid shaped ZB ZnS nanostructures are produced by using sodium sulphide as the sulphur source. It has been found that when we reduces the molar ratio of Zn to S precursor or use lower S^{2-} releasing precursor, the monomer concentration in bulk solution decreases more quickly after nucleation and hence instead of anisotropic growth, formation of spheroid or cuboid shaped nanoparticle takes place.[5-6,12,20-21] The as-synthesized nanobelts are exhibiting defect related visible PL emissions, whereas when these samples are isochronally annealed in air in the temperature range of 100^0C-600^0C white light emission is obtained. The sample obtained by annealing at 600^0C temperature is ZnO and it exhibits the PL emission of near white light having value of Commission Internationale de I'Eclairage 1931 (CIE) chromaticity coordinate of (0.30, 0.34) which is almost the same as that of white light i.e. (0.33, 0.33). UV light driven dye degradation of methyelene blue (MB) dye aqueous solution has also been demonstrated with the as-synthesized nanobelts. It shows superior performances with the degradation efficiency of ~98% within 40 min. of UV irradiation in the aqueous solution of MB dye.

2. Experimental: Materials and Methods

2.1. Synthesis of ZnS nanorods

For the synthesis of ZnS nanostructures, a teflon-lined stainless steel autoclave having 100 ml capacity has been used. All the chemicals are of analytical grade and used without any further purification. In a typical procedure, 10 mM of zinc acetate [$Zn(CH_3COO)_2$], 30 mM of thiourea [(NH_2CSNH_2)], 20 mL de-ionized (DI) water and 60mL en are taken in a beaker. Then the mixture is stirred in a magnetic stirrer for 15 min and transferred to the autoclave. After that the autoclave is sealed and heated at 220^0C for 12 h. After cooling to room temperature naturally, the products are washed with distilled water and methanol repeatedly. Finally, the products are dried at room temperature for 12h to obtain powders. A similar synthetic procedure is employed for the preparation of other samples. The products are denoted as sample S1-S5, respectively (see Table 1). For the synthesis of S1-S5 samples, we have used 10 mM of zinc acetate as the zinc precursor except for the synthesis of S4 sample for which we have used 10mM zinc nitrate as the zinc precursor.

Table 1. A brief summary of the synthesis conditions and the morphologies of the obtained samples. All the experiments were carried out at 220°C for 12h (in all experiments we have used mixture of DI water of 20 ml and en of 60 ml as solvent).

Sample Name	Sulphur source (Amount)	Phase	Morphology
S1	Thiourea (10mM)	ZB+WZ	Block-like & Belt-like
S2	Thiourea (20mM)	WZ	Belt-like
S3	Thiourea (30mM)	WZ	Belt-like
S4	Thiourea (30mM)	WZ	Belt-like
S5	Sodium sulfide (30mM)	ZB	Cuboid, Spheroid

The as-synthesized S3 sample is then annealed in air at 100^0C, 200^0C, 400^0C and 600^0C temperatures for 2h in a muffle furnace (Metrex Scientific Instruments (Pvt.) Ltd., New Delhi, India) at the heating rate of 10^0C/min and then cooled down at the same rate of 10^0C/min (furnace cooling). Henceforth, 100^0C, 200^0C, 400^0C, and 600^0C annealed S3 samples will be denoted as S3#100, S3#200, S3#400, and S3#600 respectively, unless otherwise specified.

2.2. Characterization

UV–Vis absorption spectra of the synthesized samples dispersed in DI water are recorded in the wavelength range of 200–800 nm with a double beam UV–Vis spectrophotometer (Model: Hitachi U-3010). The photoluminescence (PL) emission properties of the samples are measured at room temperature by using a photoluminescence spectrofluorimeter (Model: Perkin Elmer LS-55) equipped with pulsed Xenon discharge lamp as a source of excitation and an excitation wavelength of 330 nm is used for all the samples. For the measurement of UV-Vis absorption and PL emission spectra, equal amount of powder samples were dispersed in 20ml DI water which is then ultrasonicated for dispersion. The evaluation of phase and structure of the synthesized samples are carried out by using an X-ray diffractometer (PANLYTICAL) with Cu $K\alpha$ radiation of wavelength λ=0.15406 nm in the scan range 2θ=20^0-70^0 with a data acquisition of 0.033^0 per step. The morphologies and size of the samples are obtained by dispersing them on conducting carbon tape and observed in FEG-SEM (SIRION, FEI) equipped with an X-ray energy dispersive spectrometer (EDS). The transmission electron micrograph (TEM) images, fast Fourier transform (FFT) pattern, and high-resolution transmission electron microscope (HRTEM) images etc. are carried out on a Tecnai T-20 microscope operating at 300kV.

2.3. Photocatalytic activity studies

The UV light driven photocatalytic dye degradation activity of the as-synthesized nanobelts (S3 sample) are studied by the observation of the degradation of methyelene blue (MB) dye in aqueous medium. The experiment is carried out in a 75ml quartz reactor and a 125W medium pressure Hg lamp (Model: 3010, Photochemical reactors limited, UK) is used as the UV light source. The temperature of the reactor is controlled throughout during the experiments by circulating the water in the jacketed wall reactor. At regular time intervals the samples are taken out from the reactor, centrifuged and UV-Vis absorption spectra are monitored at the characteristics absorption peak wavelength of 664 nm of MB dye. In a typical experiment, the photocatalytic reactor is loaded with 0.02g/L MB dye and 0.015g/100mL samples. Prior to the UV light irradiation, the adsorption behaviour of MB dye with our synthesized samples are also studied. For the adsorption measurements, the dye solution loaded with the photocatalyst is stirred continuously in dark for 90 min and 2-3 ml suspension are taken out from the reactor at regular time interval. The absorbance of the sample is measured after centrifugation at the maximum absorbance wavelength of 664nm and it is found that after 30 min adsorption equilibrium is established.

3. Results and discussion

Figure 1 shows the UV-Vis absorption spectra of the synthesized materials dispersed in DI water. The UV-Vis absorption spectra of the products synthesized with different molar ratios of $Zn(CH_3COO)_2$ and thiourea are shown in Fig. 1(a) and the presences of two absorption peaks in the UV region have been observed in all samples. Earlier Fu *et al.*[22] have calculated the electronic states of $ZnSe(en)_{0.5}$ hybrid structure by density functional theory and predicted that the band-edge absorption may arise from the inorganic part or from the organic part, both being able to produce the blue shift in the absorption spectra. The appearance of the absorption peak at 223 nm, irrespective of all samples, in the present case may be due to the presence of en used during synthesis.[22] In our earlier report with $ZnS(en)_{0.5}$ nanosheets, the presences of absorption peak at 217 nm and 230 nm have been attributed to the presence of en in the complex precursor.[18] It has also been found from Fig. 1(a) that when the M_{Zn}:M_S ratio is 1:1, a broad excitonic peak appears at 331 nm, which becomes sharp and blue shifted to 323 nm and 324 nm respectively, when M_{Zn}:M_S ratio is taken as 1:2 and 1:3. The excitonic absorption peak positions in the absorption spectra of the prepared nanostructures are slightly blue shifted in compared with that of bulk ZnS (334 nm).[5] The small blue shift of the excitonic absorption peak in the UV-Vis absorption spectra has been attributed to the 'quantum confinement effect'[23] due to the extremely small thickness of the nanobelts as discussed later. Similar effect has been reported previously by Liu *et al*. in case of ZnS nanobelts.[24] The sharp absorption edges for S2 and S3 samples also indicate the relatively narrow size distribution of the synthesized nanostructures. Figure 1(b) shows the UV-Vis absorption spectra of the materials synthesized with 1:3 M_{Zn}:M_S ratio but with different zinc and sulphur precursor. For synthesis of S4 sample we have used $Zn(NO_3)_2$ and thiourea and for S5 sample we have used $Zn(CH_3COO)_2$ and Na_2S. It can be seen from Fig. 1(b) that in S3, S4, and S5 samples, the excitonic peaks have appeared at 324 nm, 325 nm, and 334 nm, respectively. In S3 and S4 sample, the excitonic peak positions are almost same because in both the cases the size of nanobelts are almost same and it is of ~ 400 nm in average length, whereas S5 sample consists of cuboid and spheroid shaped ZnS nanoparticles (shown in the SEM images later).

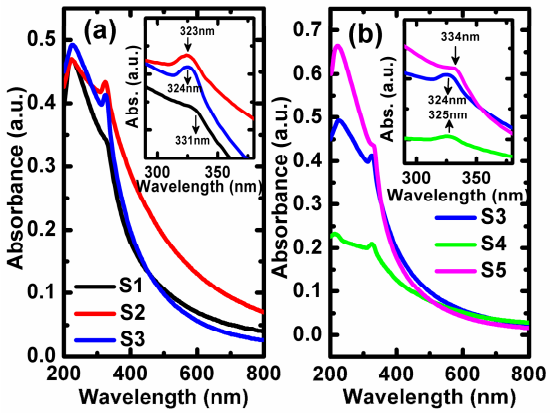

Fig. 1 UV-Vis absorption spectra of the as- synthesized samples. (a) Samples obtained by varying the molar ratio of zinc acetate to thiourea. (b) Samples obtained by using different precursor but with the same ratio of 1:3. S1, S2, and S3 sample corresponds to zinc to thiourea precursor ratio of 1:1, 1:2, and 1:3, respectively. S3, S4 and S5 samples are obtained with zinc acetate & thiourea, zinc nitrate & thiourea, and zinc acetate & sodium sulphide. Insets show the shift in excitonic peak positions.

In order to find out the changes in morphology of the synthesized products FESEM investigations of the prepared samples have been carried out. From the SEM images for the

samples synthesized with the M_{Zn}:M_S ratio of 1:1, 1:2 and 1:3 it can be found that with increasing value of molar ratio the morphology has been changed from block-like to belt-like structures, as shown in Figs. 2(a)-2(c). In case of S1 sample, most of the structures are sheet-like with some aggregated block-like structures and in case of S2 sample some broken belt-like structures are found. When the M_{Zn}:M_S ratio is increased to 1:3, almost all the structure have been converted to complete nanobelts (Fig. 2(c)). Further it can be seen from Figs. 2 (d) and 2(e) that a drastic change in morphology has been taken place when we have used different precursors but keeping the molar ratio same. It has been found that nanobelts can be

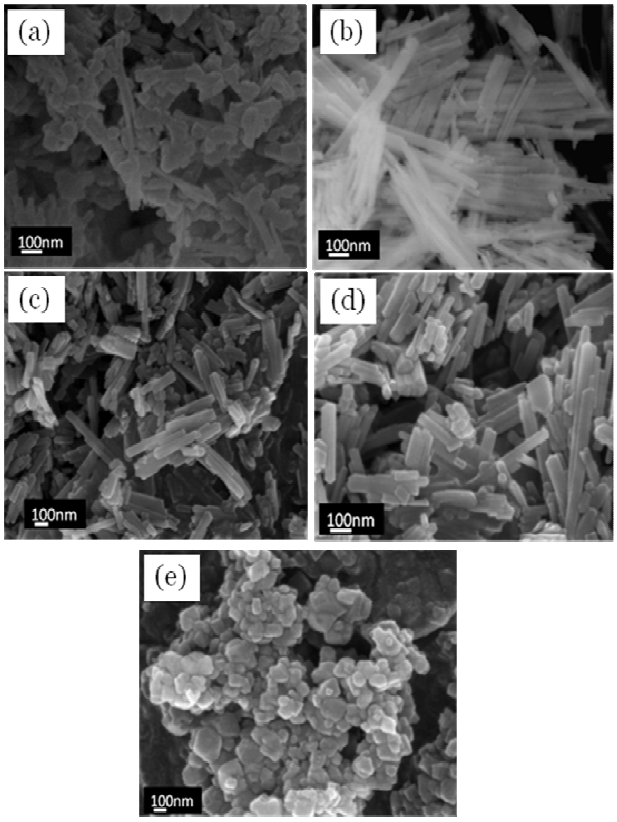

Fig. 2 The SEM images of S1-S5 samples are shown in (a)-(e).

obtained by using $Zn(NO_3)_2$ and thiourea [Fig. 2(d)], but when we use $Zn(CH_3COO)_2$ and Na_2S, spheroid and cuboid shaped ZnS nanoparticles are produced [Fig. 2(e)]. Earlier Li *et al.*[5] have also reported the synthesis of different nanostructures of ZnS by hydrothermal method and by using $Zn(NO_3)_2$ and thiourea with different molar ratios. They have obtained ZnS nanoparticles of size ~10-30 nm at a lower M_{Zn}:M_S ratio and with higher concentration they have reported the synthesis of nanorods with diameter ~10-50 nm and also hexagonal shaped nanostructures with size ~20-50 nm.

The above observations are further confirmed by TEM observations, shown in Figs. 3 and 4. At the same time, the various TEM images have been used to understand the growth direction, dimension and morphology. The high-resolution TEM (HRTEM) image is further matched with simulated atomic arrangement image using diamond software. From the TEM images of the synthesized nanostructures as shown in Fig. 3(a) for S1 sample it is clear that when the M_{Zn}:M_S ratio is 1:1, belt-like structures with some block-like structures are produced. The Selected Area Electron Diffraction (SAED) pattern taken on the block-like and belt-like structure showed the presences of ZB phase and WZ phase, respectively, further confirmed by XRD pattern analysis, presented later. A typical HRTEM image

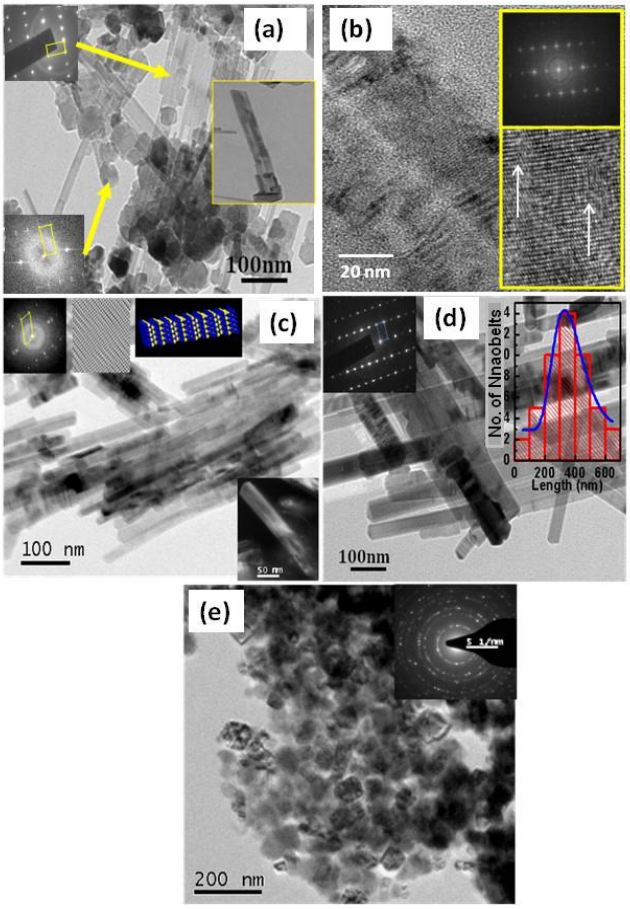

Fig. 3 TEM and HRTEM images of the as-synthesized S1 samples are shown in (a) and (b), respectively. The inset of Fig.1 (a) shows SAED pattern taken from the two individual phases. The diffraction pattern taken from block-like structure shows cubic ZnS and from belt-like structure shows hexagonal structure. The TEM image a single belt-like structure is shown in the other inset. The upper inset of (b) shows the FFT pattern of the belt-like structure showing the presence of WZ structure. The defects are shown by arrows in the lower inset of (b). The TEM images of S2, S4, and S5 samples are shown in (c), (d), and (e), respectively.

of the belt-like structures are shown in Fig. 3(b). The Fast Fourier Transform (FFT) pattern derived from the HRTEM image of the belt-like structures show that the nanobelts have been started to grow along [002] direction, as shown in the inset of Fig. 3(b). When M_{Zn}:M_S ratio is 1:2, the average length of the nanobelts is of ~400nm with width of ~5-10 nm as can be seen from Fig. 3(c). The belts are hexagonal WZ phase of ZnS as confirmed with the help of detailed analysis of TEM and HRTEM image of S2 sample. The arrangement of the atoms as obtained from the HRTEM images, shown in the inset of Fig. 3(c) clearly matches

with the simulated atomic arrangements for WZ ZnS structure. From the high angle annular dark field (HAADF) image of a single nanobelt as shown in the inset of Fig. 3(c), the uniform composition morphology of a single nanobelt has also been observed The TEM images of S4 and S5 samples are shown in Figs. 3(d) and 3(e), respectively. For S4 sample, we can see the presence of nanobelts of length ~ 400nm with a growth direction (as shown in SAED pattern in the inset) as same as previous hexagonal nanobelts, whereas for S5 sample, different shaped nanoparticles (spheroid, cuboid etc.) of average size ~100-200 nm are seen. In order to calculate the average length of the nanobelts, experimental data has been fitted with the log normal distribution as shown in the inset of Fig. 3(d). The inserted SAED pattern covering large area in the inset of Fig. 3(e) shows the presence of circular rings and those matches well with the ZB structure of ZnS.

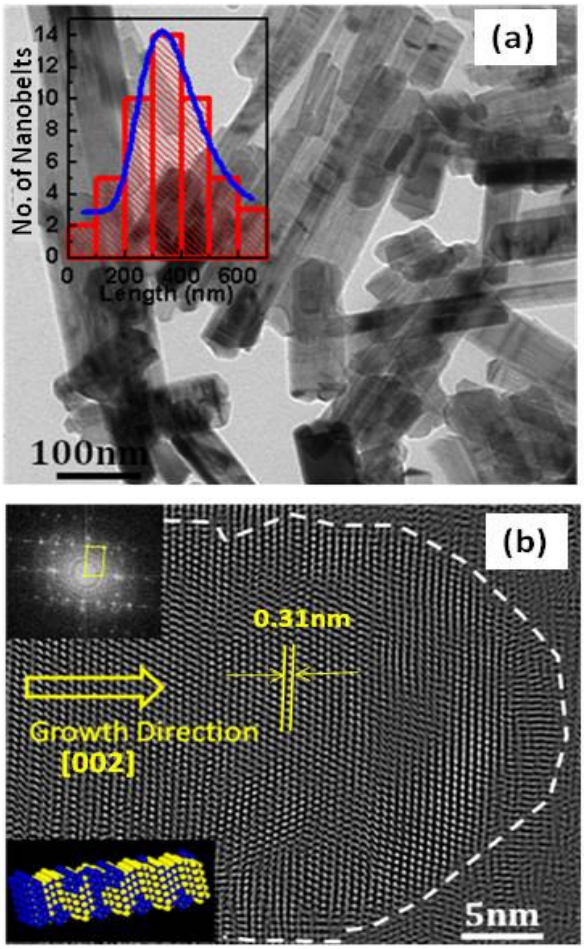

Fig. 4 Typical TEM and HRTEM images of S3 samples are shown in (a) and (b), respectively. The inset of (a) shows the distribution of length of S3 sample. (d) HRTEM image of a single nanobelt showing [002] growth direction. Inset shows Fast Fourier Transformation (FFT) pattern confirming the growth direction. The other inset shows the simulated atomic arrangements.

From the TEM image of S3 sample as shown in Fig. 4(a) it is found that when M_{Zn}:M_S is taken as 1:3 a slight increase in the length of the nanobelts (~450nm) has been taken place. The HRTEM image of S3 sample, shown in Fig. 4(b) reveals a typical single nanobelt having width of ~20 nm and the lattice spacing of 0.31 nm, corresponding to the (002) plane. The analyses of HRTEM and FFT pattern (inset of Fig. 4(b)) both confirmed that the as-obtained products are single-crystalline in nature and grow preferentially along the [002] direction, also confirmed from XRD data analyses, presented later. The sharp tip of the nanorod shows direction of growth. As shown in other inset of Fig. 4(b), the simulated atomic arrangement of the hexagonal nanorod matches well with the HRTEM observations. The presence of stacking faults in the HRTEM image of S3 sample is shown in Fig. S1 (Supplementary Information).

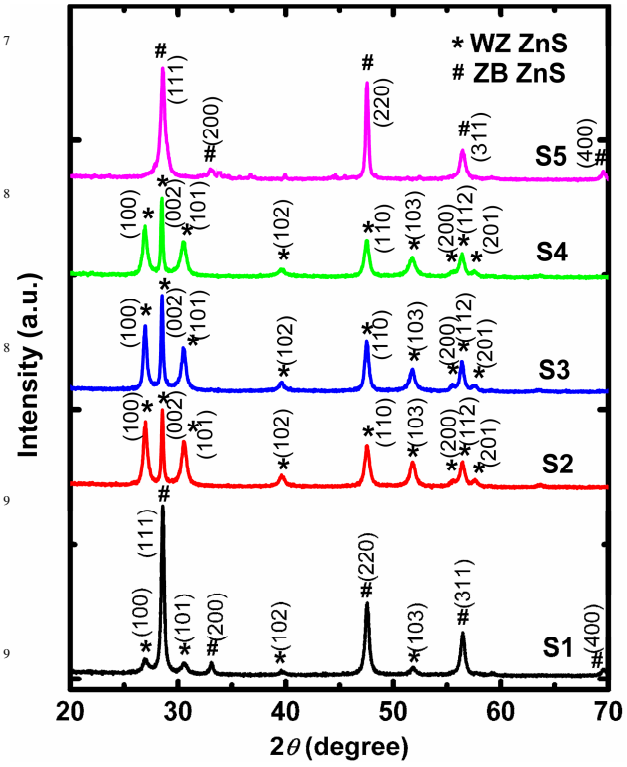

Fig. 5 XRD pattern of all as-synthesized samples. All the graphs have been rescaled to plot together.

In order to find out the information regarding the crystalline phases of the nanostructures, XRD data analyses have been performed. The XRD pattern of the synthesized materials are shown in Fig 5 which shows that all the diffraction peaks can be indexed to either ZB ZnS or WZ ZnS phase. The broadening of the XRD peaks reveals the formation of nano dimensional ZnS crystals. When M_{Zn}:M_S ratio is 1:1, a mixture of ZB and a small amount of WZ phase has been observed. The peak with 2θ values 28.70^0, 33.18^0, 47.51^0, 56.40^0, and 69.59^0 matches well with the standard Joint Committee on Powder Diffraction Standard (JCPDS) data (Card No. 80-0020) corresponding to (111), (200), (220), (311), and (400) plane of ZB ZnS. All other peak matches well with the WZ ZnS phase (JCPDS-75-1534). When the M_{Zn}:M_S ratio increases to 1:2 and 1:3, the XRD pattern reveals

the formation of pure WZ ZnS structure which has also been confirmed by the HRTEM image and FFT pattern, as discussed earlier. The highest intensity of the (002) diffraction peak compared with that of the other peaks indicate a preferential growth direction of the nanostructures along [002] direction[18,25] and has further been confirmed by HRTEM image analysis. Earlier Li *et al.*[5] have reported that during synthesis of ZnS nanostructures by hydrothermal method at 200^0C for 12h by using zinc nitrate and thiourea in 1:3 molar ratio, WZ ZnS nanorods are formed with the appearance of a very weak peak at 33.09^0 and is attributed to the diffraction of the (200) plane of the ZB phase. But in the present case when we use 1:3 molar ratio of $Zn(CH_3COO)_2$ and thiourea for hydrothermal synthesis of ZnS at 220^0C for 12h, only phase pure WZ ZnS are present. From the XRD pattern of S4 sample it has been found that by using zinc nitrate and thiourea, pure WZ ZnS phase can be formed. But if we use zinc acetate and Na_2S, we surprisingly observe that only ZB phase can be formed and it has further been confirmed by the measured SAED, as discussed earlier.

OA growth mechanism is one of the most important crystal growth mechanisms in aqueous and non-aqueous media as indicated earlier by other researchers.[6,20-21,25] Bonding between the particles reduces overall energy by removing surface energy associated with unsatisfied bonds. Before the bonding of colliding particles, there will be a rotation between the particles driven by Brownian motion and the short-range interactions between the particles to find the low-energy configuration, followed by sharing a common crystallographic orientation and joining the particles with each other.[6] During joining of the particles, in some areas of the interface lattice distortion occurs, this causes the dislocation. In the present case, on the basis of TEM and HRTEM image analyses, an OA mechanism of nanobelt formation is suggested. First, the precursor species are thermalized with the assistance of en and formation of ZnS nanocrystals (NCs) dominated by {001} basal facets and {100} side facets takes place. The {001} lattice planes of ZnS (basal facets) are polar planes composed of S anions or Zn cations.[4,6] Therefore each ZnS NCs becomes a stronger dipole along the [001] direction, which drives the OA of ZnS NCs along this direction. Further the loosely associated aggregates evolve into a single crystal by ripening, whereas there is no dipole (or electrostatic) interaction along [100] direction, which completely prevents the growth of ZnS NCs along [100] direction and ensures the formation of nanobelts.[6,20] In the present case the observed phase behaviour as well as the growth of the nanostructures with the variation of M_{Zn}:M_S ratio as well as for different precursors can be explained by the presence of both en and thiourea.[5,15-16] Ethylenediamine is well known for its template effect as it has been observed by Chen *et al.*[15] that WZ ZnS can be prepared neither in pure en solvent nor in "pure" water. It is also reported that thiourea releases S^{2-} faster in hot aqueous medium than that of Na_2S and influences alkaline conditions in the reaction mixture and consequently Zn–thiolate complex formation accelerates.[5,12,16] A fast growth rate, as discussed earlier, could lead to the anisotropy of the crystals, as WZ ZnS is an intrinsic anisotropic crystal with a preferential growth direction along the [001] direction.[4,5] As we reduce the amount of reactants or use lower S^{2-} releasing reactants, the monomer concentration in bulk solution decreases more quickly after nucleation and results in intra-particle 1D/2D ripening or normal Ostwald ripening forming spheroid or cuboid shape.[5,15].

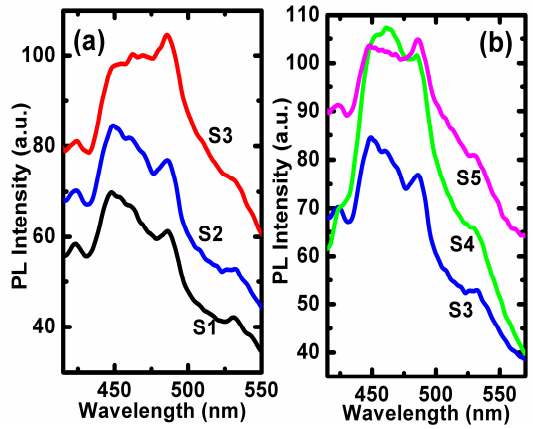

Fig. 6 PL emission spectra of the samples (measured at an excitation wavelength of 330nm) synthesized with (a) different amount of thiourea but with the same amount of zinc precursor. (b) PL emission spectra of samples synthesized with different zinc and sulphur source but with zinc to sulphur salt molar ratio of 1:3.

As the PL emission spectroscopy can provide useful information about the defects present in the nanostructures, we have performed PL emission measurements for all the samples at room temperature by dispersing them in DI water. The PL emission spectra for the samples measured at an excitation wavelength of 330 nm are shown in Figs. 6(a) and 6(b) for different M_{Zn}: M_S ratio and for different precursors, respectively. No significant change in PL emission spectra has been observed. The presence of defect related visible emission peaks has been observed in all the samples. Earlier visible PL emission from ZnS nanostructures including nanoparticles, nanorods, nanowires, nanobelts etc. have been reported by various researchers.[26-31] In the present case the emission at 423 nm is associated with the recombination of electrons at the internal sulphur vacancy (I_s) donor level with the holes trapped at the internal zinc vacancy (V_{Zn}) acceptor level.[23] The well-known blue emission peak observed at 445 nm in our samples is associated with the interstitial zinc (I_{Zn}) lattice defect, the peak at 486 nm is attributed to sulphur vacancy (V_s) related transition.[28] The origin of the green PL emission peak in ZnS nanostructures is controversial and there are several possible reasons reported behind the green emission from ZnS such as Cu-impurity related green emission at around 530 nm, and elemental S species at 535 nm.[12,29] In the present work no Cu related impurity was detected by the energy dispersive analysis of x-rays (EDAX) (not shown here) or in XRD pattern in our sample. Thus the green emission at 532nm in the present experiment might be due to elemental sulphur species as earlier observed by Ye *et al.*[29] in ZnS nanobelts.

It has been reported earlier that WZ ZnS phase could be easily transformed back to the ZB ZnS phase at ambient conditions.[11,15] Hence, the thermal stability of the synthesized WZ ZnS nanobelts

has been studied by isochronal annealing of S3 sample in air in a

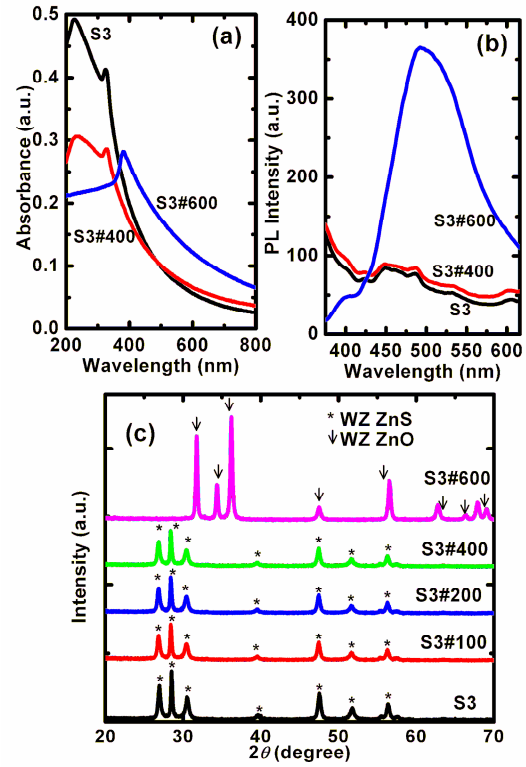

Fig. 7 (a) UV-Vis absorption spectra and (b) PL emission spectra of the samples annealed at different temperature. For the measurement of PL emission spectra an excitation wavelength of 330 nm has been used. (c) XRD pattern of the annealed samples. All the scales have been rescaled to plot together.

Muffle furnace in 100-600^{0}C temperature range for 2h. The UV-Vis absorption spectra and the PL emission spectra of the annealed S3 sample at different temperature are shown in Figs. 7(a) and 7(b), respectively. It has been found that no significant change in UV-Vis absorption spectra as well as PL emission spectra is noted when annealed at 100-400^{0}C temperature range but a drastic change is noted when the sample is annealed at 600^{0}C temperature. The excitonic peak has been red shifted from 324 nm for S3 sample to 382 nm for S3#600 sample. The appearance of an absorption peak at 382 nm indicates the formation of ZnO.[18, 30]

The formation of ZnO has also been confirmed by the XRD analyses, as shown in Fig. 7(c), which show that all the diffraction peaks appeared in case of S3#600 sample matches well with the diffraction peaks of ZnO (JCPDS-80-0075). In a recent previous report we have observed the similar phenomenon while annealing $ZnS(en)_{0.5}$ nanosheets.[18] The PL emission characteristics of S3#600 sample, measured at an excitation wavelength of 330 nm, consists of three emission peaks; (i) 397 nm peak due to near-band edge emission in ZnO, (ii) 490 nm peak due to the transition of electrons from shallow donor level formed by interstitial Zn to shallow acceptor level formed by Zn vacancies as the coexistence of these two defects has a high probability,[31] and (iii) an emission band at 514 nm which is attributed to the singly ionized oxygen vacancy in ZnO.[30-31] The CIE chromaticity co-ordinate for S3#600 sample has been calculated, as shown in Fig. 8, from the measured PL spectra, and it is found out to be (0.30, 0.34), which is very close to that of white light (0.33, 0.33). It is expected that these results will open up new possibilities for applications of the synthesized materials in white light emitting devices.

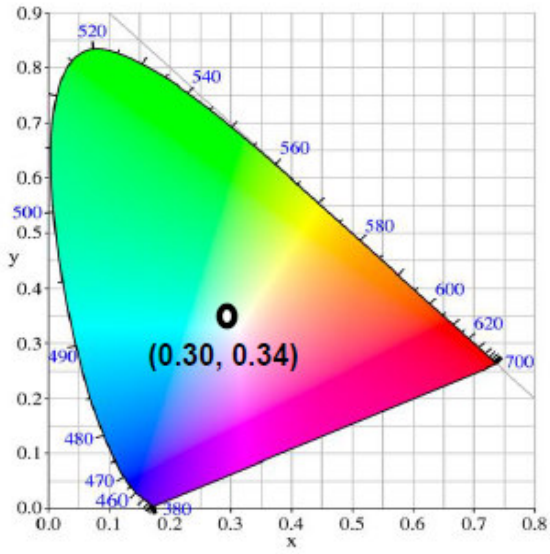

Fig. 8 CIE chromaticity co-ordinate of S3#600 sample, produced by annealing S3 at 600^{0}C temperature for 2h.

It has been found that the as-synthesized ZnS nanobelts, viz. S3 sample, are exhibiting superior performances as photo-catalyst for photo degradation of MB dye under UV light irradiation. The intensity of the characteristics absorbance peak of MB dye appeared at ~ 664 nm has been used for monitoring the adsorption and photocatalytic degradation of the dye. Prior to UV-light irradiation, adsorption measurements are performed. It has been found that the adsorption equilibrium is obtained after 30 min and the obtained value of adsorption is found out to be ~10%. The experimentally obtained absorption spectra of MB dye, taken at different irradiation time, in presence of the S3 sample are shown in Fig. 9(a). It is found that the intensity of absorption peak that appeared at 664 nm has been diminished gradually with increasing irradiation time. No new absorption bands appeared which indicates the complete photo degradation of MB dye. Upon UV irradiation, the colour of the MB dye solution, in presence of ZnS nanobelts, is found out to be rapidly degraded with time, and the corresponding digital photographs are also taken which are shown in the inset of Fig. 9(a).

The degradation efficiency of dye has been calculated by using the formula, MB degradation (%) = 100× (C_0-C)/C_0, where C_0 is the initial concentration and C is the concentration of the MB dye at any time t, respectively.[32-36] In order to calculate accurately the MB degradation efficiency we have performed the baseline correction and Gaussian deconvolution of the overlapped absorption bands. We have followed the method as illustrated by Marbán *et al.*[37]and similar method has been used earlier by Siqueira *et al*. in case of MB dye degradation analysis by using bismuth sulphide and zinc sulphide photocatalyst.[38-39] The total visible spectrum of MB dye has been deconvoluted into three Gaussian peaks (588nm, 618nm, and 664nm) as shown in the

inset of Fig. 9(b) for MB dye after 40 min irradiation, viz. as an example. The MB dye concentration (C) is related to the absorbance of peak at 664 nm (A_{664}) by using the equation, $C = 0.407A_{664}^2 + 4.319A_{664}$, where, $A_{664} = \frac{f_{664}}{\sigma_{664}\sqrt{2\pi}} A_T$, A_T is the total area of the visible spectrum before normalisation, f_{664} is the normalized area of the 664 nm peak, and σ_{664} is the standard deviation of the Gaussian fitted peak at 664 nm.[37] As shown in Fig. 9(a), it is clear that the MB dye solution becomes almost colourless after irradiation for only 40 min. with the degradation efficiency of ~98%, indicating the superior performance of the synthesized ZnS nanobelts for photo-degradation of MB dye.

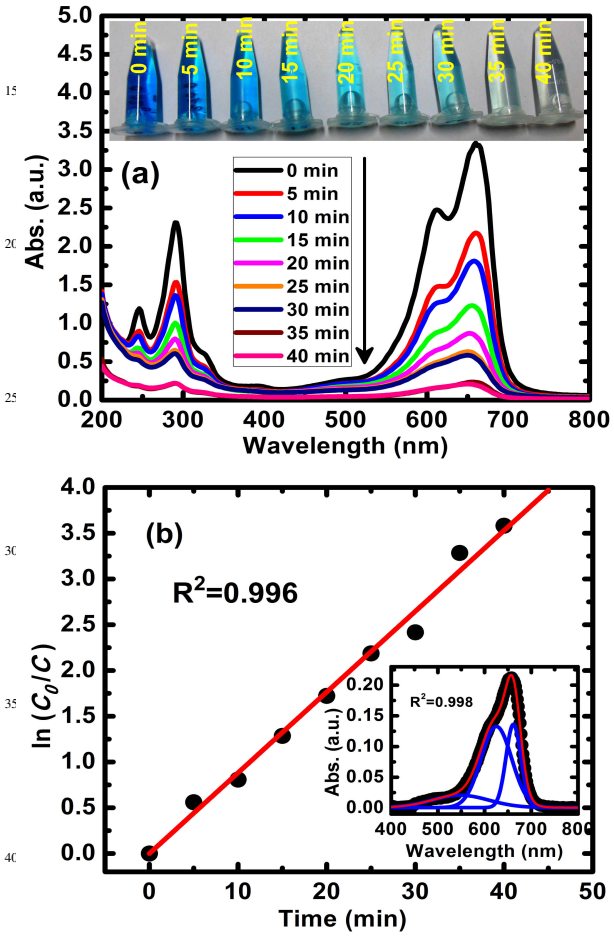

Fig. 9 (a) UV-Vis absorption spectra of MB dye solution collected at different time intervals after addition of S3 sample and after irradiation of UV light. It may be noted that before UV light irradiation dye and S3 sample mixture has been stirred for 30 min in dark. The inset shows the colour change in the sample with time. (b) Degradation kinetics has been fitted with pseudo-first order kinetic reaction model. Inset shows the baseline corrected absorption spectra (symbols) of the sample irradiated for 40 min deconvoluted with three Gaussian peaks (blue line) and the resultant spectrum is shown by red line.

In order to quantitatively understand the reaction kinetics of MB dye degradation, the experimental data have also been further analysed as shown in Fig. 9(b) and it is found that it is following pseudo-first order kinetic model, expressed as $ln\ (C_o/C) = kt$.[18,34-35] Here, C_o is the initial concentration, C is the concentration of the dye at any time t and k is the reaction rate constant and it has been found that the reaction constant is 0.088min^{-1} (R^2=0.996). Such pseudo-first order kinetic reaction model has also been by earlier authors and it is generally used to explain the photocatalytic degradation reactions which take place at the interface between the catalysts and the organic pollutants with low concentration.[33-34] As the synthesized ZnS nanorods absorbs UV light very strongly, electron-hole pairs are generated in the upon irradiation of UV light in the photo-catalyst material, i.e. in ZnS, which further led to the degradation of dye molecules.[31-34,40]

Conclusions

In this work, we have attempted synthesis of ZnS nanostructures of different morphologies, such as block-like, belt-like, spheroid and cuboid shaped nanoparticles by using the simple hydrothermal technique. It has been shown that the tailoring of both the phase and shape of ZnS nanostructures are easily possible by controlling the amount of sulphur precursor or by using different types and ratio of zinc and sulphur precursors. The synthesis of phase pure WZ ZnS nanobelts having average length of ~400nm and diameter of ~10-20nm has been demonstrated at 220^{0}C temperature, which is much lower than the cubic to hexagonal phase transition temperature of 1020^{0}C required for bulk ZnS. The observed shape evolution of the synthesized nanostructures has been explained by using the mechanism of oriented attachment growth. It has been also been found that 1:3 molar ratio of zinc to sulphur source is required to obtain pure WZ ZnS belt-like structures. An increase in sulphur concentration leads to faster growth of ZnS NCs along [001] direction and formation of belt-like structure has taken place. Defect related visible PL emissions are observed from the synthesized samples and when the nanobelts are annealed at 600^{0}C temperature, almost white light emission, with a calculated CIE colour coordinate of (0.30, 0.34), is obtained. The synthesized nanobelts have been shown to exhibit superior performances for degradation of MB dye and with dye degradation efficiency ~98% within 40 min of UV light irradiation. The present investigation has provided a method to fabricate ZnS nanocrystals with controllable phases and morphologies having potential applications in cleaning of waster water by degradation of dye molecules dissolved in water as well as in white light emitting device fabrication in near future.

Acknowledgements

Authors are grateful to Department of Science and Technology (SR/FTP/PS-67/2008), Government of India, for the partial financial support. AKK is grateful to the Ministry of Human Resource Development (MHRD), National Institute of Technology Durgapur, India for the maintenance scholarship. AKK is also grateful to UGC, GOI, for providing the financial support during the visit to the Networking Resource Centre for Materials (NRCM), Indian Institute of Science (IISc), Bangalore. Authors are also thankful to Dr. R. N. Saha and Mr. T. Mallick, Dept. of Chemistry, NIT, Durgapur for allowing us to use UV light driven photocatalytic activity set-up.

[a] *Nanoscience Laboratory, Department of Physics, National Institute of Technology, Durgapur-713209, West Bengal, India*
[b] *Department of Materials Engineering, Indian Institute of Science, Bangalore, 560012, India*
* *Corresponding author E mail: pathik.kumbhakar@phy.nitdgp.ac.in & nitdgpkumbhakar@yahoo.com*
Tel.:-+91-343-2546808, Fax:-+91-343-2547375

References

1 X. Fang, T. Zhai, U. K. Gautam, L. Li, L. Wu, Y. Bando and D. Golberg, *Prog. Mater. Sci.,* 2011, **56**, 175.
2 X. Fang, L. Wu and L. Hu, *Adv. Mater.,* 2011, **23**, 585.
3 W. T. Yao, S. H. Yu and Q. S. Wu, *Adv. Funct. Mater.,* 2007, **17**, 623.
4 D. Moore and Z. L. Wang, *J. Mater. Chem*., 2006, **16**, 3898.
5 Z. Li, B. Liu, X. Li, S. Yu, L. Wang, Y. Hou, Y. Zou, M. Yao, Q. Li, B. Zou, T. Cui, G. Zou, G. Wang and Y. Liu, *Nanotechnology,* 2007, **18**, 255602.
6 G. Zhu, S. Zhang, Z. Xu, J. Ma and X. Shen, *J. Am. Chem. Soc.,* 2011, **133**, 15605.
7 J. Lu, X. Zeng, H. Liu, W. Zhang and Y. Zhang, *Appl. Surf. Sci.,* 2012, **258**, 8538.
8 M. Hafeez, T. Zhai, A. S. Bhatti, Y. Bando and D.Golberg, *J. Phys. Chem. C,* 2012, **116**, 8297.
9 Z. G. Chen, L. Cheng, H. Y. Xu, J. Z. Liu, J. Zou, T. Sekiguchi, G. Q. Lu and H. M. Cheng, *Adv. Mater.,* 2010, **22**, 2376.
10 A. K. Kole, P. Kumbhakar and U. Chatterjee, *Chem. Phys. Lett.*, 2014, **591**, 93.
11 Z. Wang, L. L. Daemen, Y. Zhao, C. S. Zha, R. T. Downs, X. Wang, Z. L.Wang and R. J. Hemley, *Nature Mater*., 2005, **4**, 922.
12 S. Biswas and S. Kar, *Nanotechnology,* 2008, **19**, 045710.
13 S. A. Acharya, N. Maheshwari, L. Tatikondewar, A. Kshirsagar and S. K. Kulkarni, *Cryst. Growth Des.,* 2013, **13**, 1369.
14 G. Xi, C. Wang, X. Wang, Q. Zhang and H. Xiao, *J. Phys. Chem. C,* 2008, **112**, 1946.
15 X. Chen, H. Xu, N. Xu, F. Zhao, W. Lin, G. Lin, Y. Fu, Z. Huang, H. Wangand and M.Wu, *Inorg. Chem.,* 2003, **42**, 3100.
16 Z. X .Deng, L. Li and Y. Li, *Inorg. Chem.,* 2003, **42**, 2331.
17 L. Nasi, D. Calestani, T. Besagni, P. Ferro, F. Fabbri, F. Licci and R. Mosca, *J. Phys. Chem. C,* 2012, **116**, 6960.
18 A. K. Kole, C. S. Tiwary and P. Kumbhakar, *CrystEngComm.,* 2013, **15**, 5515.
19 W. Liu, N. Wang, and R. Wang, *Nano Lett.* 2011, **11**, 2983.
20 Y. Liu, J. Hu, T. Zhou, R. Che and J. Li, *J. Mater. Chem*., 2011, **21**, 16621.
21 P. Thangadurai, S. Balaji and P. T. Manoharan, *Mater. Chem. Phys*., 2009, **114**, 420.
22 H. Fu and J. Li, *J. Chem. Phys.,* 2004, **120,** 6721.
23 L. Brus, *J. Phys. Chem.,* 1998, **90**, 2555.
24 W. Liu, R. Wang, and N. Wang, *Appl. Phys. Lett.* 2010, **97**, 041916 .
25 X. Wang, Q. Zhang, B. Zou, A. Lei and P. Ren, *Appl. Surf. Sci.,* 2011, **257**, 10898.
26 D. Denzler, M. Olschewski and K. Sattler, *J. Appl. Phys.,* 1998, **84**, 2841.
27 X. Wang, J. Shi, Z. Feng, M. Lia and C. Li, *Phys. Chem. Chem. Phys.,* 2011, **13**, 4715.
26 H. Tang, G. Xu, L. Weng, L. Pan and L. Wang, *Acta Materialia,* 2004, **52**, 1489.
27 C. Ye, X. Fang, G. Li and L. Zhang, *Appl. Phys. Lett.,* 2004, **85**, 3035.
28 N. Kumbhojkar, V. V. Nikesh, A. Kshirsagar and S. Mahamuni, *J. Appl. Phys.,* 2000, **88**, 6260.
29 D. A. Reddy, D. H. Kim, S. J. Rhee, C. U. Jung, B. W. Lee and C. Liu, J Alloy Compds., 2014, **588**, 596.
30 Y. W. Chen, Y. C. Liu, S. X. Lu, C. S .Xu and C. L. Shao, *J. Chem. Phys.,* 2005, **123**, 134701.
31 X. M. Fan, J. S. Lian, L. Zhao and Y. H. Liu, *Appl. Surf. Sci.,* 2005, **252**, 420.
32 H. R. Pouretedala, A. Norozib, M. H. Keshavarza, A. Semnanic, *J. Hazard. Mater.,* 2009, **162**, 674.
33 S. Ma, R. Li, C. Lv, W. Xu and X. Gou, *J. Hazard. Mater.,* 2011, **192**, 730.
34 S. K. Kansal, M. Singh and D. Sud, *J. Hazard. Mater.*, 2007, **141**, 581.
37 G. Marbán, T. T. Vu, and T. V. Solís, Appl. Catal., A, 2011, **402**, 218.
38 G. O. Siqueira, A. de O. Porto, M. M. Viana, H. V. da Silva, Y. G. de Souza, H. W. A. da Silva, G. M. de Lima and T. Matencio, *Phys.Chem. Chem. Phys*., 2013, **15**, 16236.
39 G. O. Siqueira, T. Matencio, H. V. da Silva, Y. G. de Souza, J. D. Ardisson, G. M. de Limaa and A. de Oliveira Porto, *Phys.Chem. Chem. Phys.,* 2013, **15**, 6796.
40 M. A. Behnajady, N. Modirshahla and R. Hamzavi, *J. Hazard. Mater. B,* 2006, **133**, 226.

Graphics for Table of Contents